An Automotive Onboard AC Heater Without External Power Supplies for Lithium-Ion Batteries at Low Temperatures

Yunlong Shang, *Student Member, IEEE*, Bing Xia, *Student Member, IEEE*, Naxin Cui, *Member, IEEE*, Chenghui Zhang, *Senior Member, IEEE*, and Chunting Chris Mi, *Fellow, IEEE*

***Abstract*—In cold climates, lithium-ion batteries suffer severe power/energy loss, bad performance, and reduced life cycle. Many internal ac heating strategies have been proposed to provide fast heating with a higher efficiency and better uniformity. However, the ac current is typically generated by an offboard equipment with grid power supply, which is a main bottleneck of the ac heating applied to electric vehicles. Therefore, an automotive onboard ac heater is proposed to heat lithium-ion batteries at low temperatures without the requirement of external power supplies. Only one pair of complementary pulse width modulation signals is employed to drive the proposed ac heater, and the heating speed can be online regulated by controlling the switching frequency. Particularly, the heating time can be reduced drastically by combining two heaters in interleaved parallel without causing harm to the batteries. In addition, the heating circuit can also realize the automatic balancing for battery cells if needed. Experimental results show that the proposed interleaved parallel heater, by circulating an ac current with the amplitude of 3.1 C and the frequency of 833 Hz, can heat lithium-ion batteries from −20 to 0 °C within 5.9 min, consuming about 5% of cell energy.**

***Index Terms*—Battery equalizers, battery heaters, battery management systems (BMSs), buck–boost converters, electric vehicles (EVs).**

Manuscript received June 11, 2017; revised September 6, 2017; accepted October 24, 2017. Date of publication October 31, 2017; date of current version June 22, 2018. This work was supported in part by the Major Scientific Instrument Development Program of the National Natural Science Foundation of China under Grant 61527809, in part by the Key Project of National Natural Science Foundation of China under Grant 61633015, and in part by the U.S. Department of Energy under the Graduate Automotive Technology Education Center program. Recommended for publication by Associate Editor M. Ferdowsi. *(Corresponding author: Chenghui Zhang.)*

Y. Shang is with the School of Control Science and Engineering, Shandong University, Shandong 250061, China, and also with the Department of Electrical and Computer Engineering, San Diego State University, San Diego, CA 92182 USA (e-mail:shangyunlong@mail.sdu.edu.cn).

B. Xia is with the Department of Electrical and Computer Engineering, San Diego State University, San Diego, CA 92182 USA, and also with the Department of Electrical and Computer Engineering, University of California San Diego, La Jolla, CA 92093 USA (e-mail: bixia@eng.ucsd.edu).

N. Cui and C. Zhang are with the School of Control Science and Engineering, Shandong University, Jinan 250061, China (e-mail: cuinx@sdu.edu.cn; zchui@sdu.edu.cn).

C. C. Mi is with the Department of Electrical and Computer Engineering, San Diego State University, San Diego, CA 92182 USA (e-mail: cmi@sdsu.edu).

Color versions of one or more of the figures in this paper are available online at http://ieeexplore.ieee.org.

Digital Object Identifier 10.1109/TPEL.2017.2768661

I. Introduction

ELECTRIC vehicles (EVs) have been rapidly developed in recent years, driven by the urgency to conserve energy and to protect the environment [1]. However, in cold weather conditions, the driving range of EVs will drop substantially due to the drastic increase in internal resistances of lithium-ion batteries at low temperatures, causing severe loss of usable energy and power [2]–[4]. For example, a commercial 18650 lithium-ion battery only offers 5% of energy and 1.25% of power at –40 °C compared with that at 20 °C [5]. More severely, battery degradation will be accelerated due to the operation for batteries at subzero temperature causing lithium plating [6], [7]. Therefore, heating onboard batteries of EVs has become a pressing need to improve the driving range of EVs in cold temperatures, which is a thriving research area [8]–[10].

Many heating approaches have been reported in the literatures, which can be classified into two groups: external heating and internal heating [11]–[22]. According to the heating medium, external heating can be further divided into air heating and fluid heating [11]. External heating methods usually need many electric resistance wires wrapped outside batteries using air or liquid as the medium to heat batteries, leading to a lot of heat diffusing to the environment [12]–[14]. Moreover, external heating has the severe problem of heating nonuniformity because of the heat diffusion, accelerating the aging of some batteries [12]. In summary, external heating methods have the critical disadvantages of large size, heavy weight, high cost, nonuniformity, and energy loss to the environment, leading to a slow heating speed and low efficiency.

In contrast, the internal heating methods can heat batteries utilizing the real part of battery impedances during charging and discharging rather than using external heaters, eliminating the long paths of heat conduction and avoiding the heat diffusion to the environment [11], [12]. The internal heating can be further divided into the direct-current (dc) and alternating-current (ac) methods [12]. For the dc heating method, the current amplitude and duration should be within certain limits to avoid lithium deposition, thereby leading to a low heating generation rate and bad preheating effectiveness [11], [12]. By comparison, the ac heating method can heat batteries by alternatingly charging and discharging batteries, which avoids substantial change of the state-of-charge (SOC) and lithium deposition [12]. In

conclusion, the internal ac heating method will be much more effective and has the potential to provide a faster heating with a higher efficiency and uniformity.

Ji and Wang [12] proposed several heating strategies for lithium-ion batteries and showed that a high-frequency ac signal with a large amplitude could speed up the heating process. Vlahinos and Pesaran [15] showed that applying an ac current to the battery terminals was a feasible way to heat batteries and the internal heating had a faster speed and better uniformity than external heating. Pesaran *et al.* [16] provided an overview of battery preheating methods and showed that the ac heating is the most effective way to warm batteries at cold temperatures. Zhang *et al.* [17] developed an internal ac heating method with low frequencies for cells at low temperatures, and showed that the ac amplitude and frequency had significant impact on the heat generation rate. Moreover, they concluded that the ac heating method had little damage to the battery health. Ruan *et al.* [18] proposed a rapid and effective internal heating strategy for batteries at low temperatures, and derived the optimal frequency for maximum heat generation rate. Wang *et al.* [19] reported an "all-climate" lithium-ion battery structure that could heat itself up from below 0 °C. It only took 20 and 30 s to heat the battery from –20 °C and –30 °C to 0 °C, consuming only 3.8% and 5.5% of cell capacity, respectively. Then, Zhang *et al.* [20] reported the improved self-heating lithium-ion battery that can be heated from –20 °C to 0 °C within 12.5 s, consuming 24% less energy than that reported previously. Yang *et al.* [21] developed an electrochemical-thermal coupled model for self-heating Li-ion batteries to predict the internal characteristics of batteries, and showed the heating time and energy consumption would be greatly affected by internal temperature gradient. Stuart and Hande [22] designed a high-frequency converter using IGBTs and diodes to heat NiMH batteries in hybrid electric vehicles (HEVs) at low temperatures. However, the control was extremely complex due to the measurement of the accurate zero-crossing point of current. Particularly, the converter was supplied by the onboard generator driven by the HEV's heat engine, which could not be applied to EVs. Moreover, the authors commented that it was not feasible for batteries to provide enough energy to heat themselves.

It is important to note that the energy source to heat onboard batteries is the major challenge of battery heating [11], [12]. Generally, the potential heat sources could be engines, generators, batteries, and external power supplies [11]. Obviously, only HEVs can utilize the heat and power from the onboard engines and generators to heat batteries, but leading to a slow heating speed. Nonetheless, for EVs without engines and generators, only the energy in batteries or offboard chargers can be used to warm batteries electrically. Ji and Wang [12] developed the external convective heating and the internal dc heating only using the energy in batteries. Although these two methods do not require external power supplies, which enable a low cost and high reliability, these strategies suffer from low heating efficiency, long heating time, and large battery capacity loss [12]. As aforementioned, the internal ac heating is a preferred method since it shows good heating performances with faster speeds, higher efficiency, better uniformity, and little damage to battery cycle life [11], [12]. However, the ac current for heating batteries is usually generated by an offboard equipment with a bulky volume and heavy weight supplied by the power grid, which is the main drawback of the internal ac heating methods applied to EVs. So far, there is still not an efficient automotive onboard ac heater with a small size and low cost, particularly, without the requirement of additional power supplies. This paper aims to address the difficult implementation issue of the internal ac heating methods for the onboard batteries used in EVs at low temperatures. It is first proved that it is fully feasible for batteries to provide enough energy to heat themselves without the requirements of any external power supplies and devices, leading to an easy implementation of the ac heating method for EVs. The proposed heater only needs one pair of complementary pulse width modulation (PWM) signals to drive MOSFET switches without the requirement of any sensing circuit, leading to a simple control. Furthermore, the heating speed can be easily regulated by controlling the switching frequency, making the proposed heater to possess a wide adaptability. Particularly, the proposed heater can also be used to automatically balance cell voltages with the same control at a higher frequency without the requirement of additional balancing circuits. In summary, the proposed system has the inherent advantages of the small size, low cost, simple control, high efficiency, fast speed, good uniformity, and high reliability. Therefore, the proposed method can solve effectively the subzero-temperature and unbalanced-voltage issues of rechargeable batteries, by which "all-climate" and "all-voltage" batteries can be easily achieved without the need of redesigning new battery structures, being of great significance to the rapid development of EVs.

II. Proposed AC Heater

In this paper, an onboard ac heater based on buck–boost conversion is proposed, which is a simple implementation of the ac heating strategies [11], [12] applied to EVs.

A. Configuration of Proposed AC Heater

The purpose of the proposed heater is to produce an ac current without the need of external power supplies to alternately charge and discharge batteries, by which the batteries can be self-heated by the ohmic losses, *i.e.*, $I^2 R_{\rm B}$. Fig. 1(a) shows the proposed basic heating topology, where only one buck–boost converter is applied to the whole battery pack, which is divided into two parts, without the requirement of additional power supplies. This structure needs less components with a smaller size and lower cost, but only takes half time to alternately heat the two parts of the batteries, leading to a slow heating speed and low efficiency. In order to achieve the simultaneous heating for the upper and lower cells to improve the heating speed and efficiency, the "all-time" interleaved parallel structure of battery heater is proposed, as shown in Fig. 1(b). A second buck–boost converter is added in parallel to the first topology. The two conversion units are interleaved with 180° phase shift angle under a duty cycle of ideally 50%. Thus, this interleaved parallel structure can effectively heat batteries all the time, which is very favorable to increase the rms heating

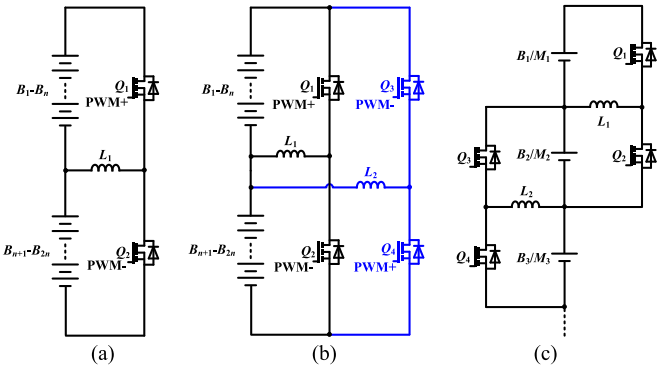

Fig. 1. Proposed ac heaters. (a) The proposed basic heater using one buck–boost converter. (b) The improved topology 1—the "all-time" interleaved parallel heater. (c) The improved topology 2—the next-to-next heater with balancing function. Note: $B_1, B_2, B_3, \ldots$ represent battery cells, and $M_1, M_2, M_3, \ldots$ represent battery modules.

current with the same current amplitude as the basic topology. Therefore, this "all-time" topology not only achieves a higher heating speed and efficiency but also has no more damage to batteries compared with the first method. Fig. 1(c) shows the improved "next-to-next" topology with one buck–boost converter set for two adjacent cells/modules. Due to the 1:1 conversion ratio of the buck–boost converter at 50% duty cycle, energy will flow automatically from the higher voltage cell to the adjacent lower voltage one [23]. Therefore, except battery heating, this structure can also achieve the balancing among cells or modules at higher frequencies [23]. The main limitation of this approach is the increase of the number of components, which may appear more complex to implement. Nevertheless, on the one hand, because the required power of each component decreases drastically, the size of each component can be reduced significantly. On the other hand, this topology can achieve the equalization for cells or modules at a higher frequency without the need of additional balancing circuits, consequently increasing the power density. Actually, these changes simplify the integration and the implementation of the proposed next-to-next topology. In summary, the above three methods can help manufacturers to select, optimize, and implement viable heating topologies according to different applications.

The proposed heating solutions have some favorable features as follows:

1) The proposed heater is based on buck–boost conversion. For the basic topology, only two MOSFET switches and one inductor are needed for the whole battery pack, leading to a smaller size and lower cost compared with the external heating methods [11], [12].
2) Only one pair of complementary PWM signals is employed to drive the proposed heaters without the need of cell voltage and current monitoring, leading to the ease of control.
3) With the proposed system, batteries can heat themselves up from below 0 °C without requiring external heating devices and power supplies, resulting in simple implementation in EVs.
4) The heating speed can be regulated online by controlling the switching frequency with a good flexibility.
5) The heating speed and efficiency can be improved drastically by combining the proposed basic heaters in interleaved parallel without causing more harm to batteries.
6) The proposed next-to-next topology contains two functions, *i.e.*, heating with a lower frequency and balancing with a higher frequency, increasing the power density of battery management systems (BMSs).
7) Due to the small size and ease of control, the proposed heater can be easily integrated into battery packs, by which "all-climate" and "all-voltage" batteries are immediately achieved without the need of changing battery structures and electrolytes.
8) The proposed ac heaters can be applied to other rechargeable batteries without any change or recalibration, such as nickel–cadmium batteries, lead-acid batteries, and nickel-metal-hydride batteries.

B. Operation Principles

In order to simplify the analysis for the operation modes, the basic heater is applied to two cells connected in series, *i.e.*, B_1 and B_2, as shown in Fig. 2. The batteries are modeled as an internal resistance R_B and a voltage source V_{OC} connected in series. The terminal voltage of the battery is represented by V_B. The proposed heater is driven by a pair of complementary PWM signals, *i.e.*, PWM+ and PWM–, and has four steady working modes in one switching period. The four working modes are operated alternatively and an ac current is automatically circulated between the two cells. Figs. 2 and 3 show the operating modes and theoretical waveforms of the proposed battery heater, respectively.

It is assumed that the battery cells have the same terminal voltage and the same internal resistance

$$V_B = V_{B1} = V_{B2} \tag{1}$$

$$R_B = R_{B1} = R_{B2}. \tag{2}$$

The MOSFETs have the same static drain source on resistance

$$R_{\mathrm{DS(on)}} = R_{\mathrm{DS(on)},Q1} = R_{\mathrm{DS(on)},Q2}. \tag{3}$$

The equivalent resistance R_1 in Fig. 2 represents the total resistances of the inductor L_1 and one MOSFET switch, which can be given by

$$R_1 = R_{L1} + R_{\mathrm{DS(on)}} \tag{4}$$

where R_{L1} is the equivalent resistance of the inductor L_1.

1) Mode I [$t_0 - t_1$, Fig. 2(a)]: At t_0, Q_1 is turned ON, and Q_2 is turned OFF. Cell B_1 is charged by inductor L_1, thus, the inductor current i_L begins to decrease. Based on Kirchhoff's current law (KCL), i_L can be deduced as

$$i_L(t) = i_L(t_0) - \frac{V_{B1}}{R_1}\left(1 - e^{-\frac{R_1}{L_1}(t-t_0)}\right). \tag{5}$$

At t_1, inductor current i_L drops to 0. By solving (5), the duration of Mode I $t_1 - t_0$ can be calculated as

$$t_1 - t_0 = -\frac{L_1}{R_1}\ln\left[1 - \frac{R_1}{V_{B1}} \cdot i_L(t_0)\right]. \tag{6}$$

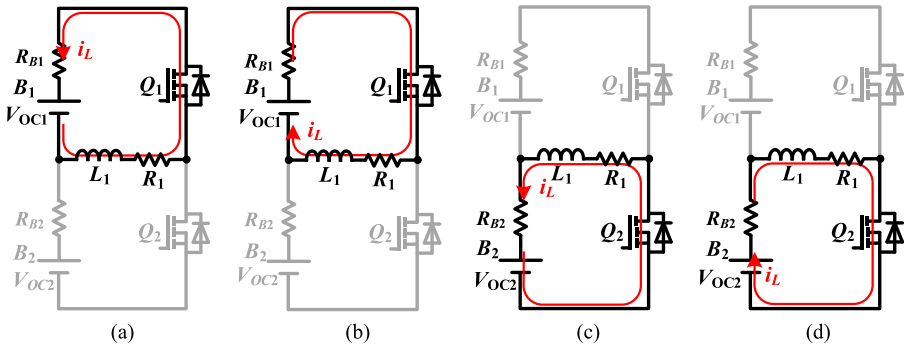

Fig. 2. Operating modes of the proposed ac heater for two battery cells. (a) Mode I. (b) Mode II. (c) Mode III. (d) Mode IV.

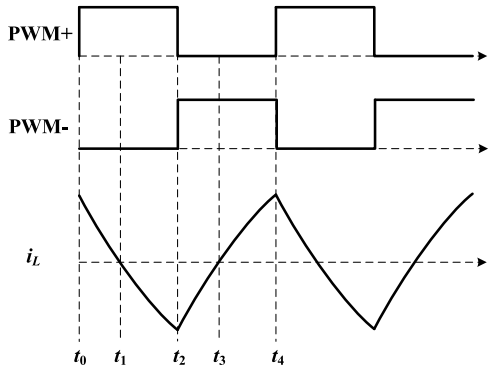

Fig. 3. Key waveforms of the proposed ac heater.

Based on (5) and (6), the energy consumed by the internal resistance R_{B1} during Mode I can be approximatively given by

$$E_{R_{B1}}(\mathrm{I}) \approx \left[\frac{1}{2}\cdot i_L(t_0)\right]^2 \cdot R_{B1}\cdot(t_1-t_0) = -\frac{1}{4}\cdot L_1\cdot\frac{R_{B1}}{R_1}\cdot i_L^2(t_0)\cdot\ln\left[1-\frac{R_1}{V_{B1}}\cdot i_L(t_0)\right]. \quad (7)$$

Analogously, the energy consumed by the equivalent resistance R_1 during Mode I can be given by

$$E_{R1}(\mathrm{I}) \approx -\frac{1}{4}\cdot L_1\cdot i_L^2(t_0)\cdot\ln\left[1-\frac{R_1}{V_{B1}}\cdot i_L(t_0)\right]. \quad (8)$$

It is important to note that the maximum energy stored in the inductor L_1 at t_0 can be expressed as

$$E_{L1}(t_0) = \frac{1}{2}\cdot L_1\cdot i_L^2(t_0). \quad (9)$$

2) Mode II [$t_1 - t_2$, Fig. 2(b)]: Q_1 keeps being turned ON, and Q_2 keeps being turned OFF. When the inductor current i_L decreases to 0 at t_1, Mode II starts. Cell B_1 transfers energy to inductor L_1, and then inductor current i_L rises reversely. During this mode, i_L can be represented by

$$i_L(t) = -\frac{V_{B1}}{R_1}\left(1-e^{-\frac{R_1}{L_1}(t-t_1)}\right). \quad (10)$$

Like Mode I, the energy consumed by R_{B1} during Mode II can be approximatively expressed as

$$E_{R_{B1}}(\mathrm{II}) \approx -\frac{1}{4}\cdot L_1\cdot i_L^2(t_2)\cdot\frac{R_{B1}}{R_1}\cdot\ln\left[1+\frac{R_1}{V_{B1}}\cdot i_L(t_2)\right]. \quad (11)$$

The energy consumed by R_1 during Mode II can be given by

$$E_{R1}(\mathrm{II}) \approx -\frac{1}{4}\cdot L_1\cdot i_L^2(t_2)\cdot\ln\left[1+\frac{R_1}{V_{B1}}\cdot i_L(t_2)\right]. \quad (12)$$

Thus, based on (7) and (11), considering that R_1 is smaller, the total energy used for heating B_1 during one switching period can be approximatively deduced as

$$E_{R_{B1}} \approx \frac{1}{4}\cdot\frac{L_1}{V_{B1}}\cdot R_{B1}\cdot[i_L^3(t_0)-i_L^3(t_2)]. \quad (13)$$

It can be found that the heating speed of B_1 is proportional to the ac amplitudes $i_L(t_0)$ and $i_L(t_2)$ as well as the internal resistance R_{B1}.

The maximum energy stored in the inductor L_1 at t_2 can be obtained as

$$E_{L1}(t_2) = \frac{1}{2}\cdot L_1\cdot i_L^2(t_2). \quad (14)$$

3) Mode III [$t_2 - t_3$, Fig. 2(c)]: At t_2, Q_2 is turned ON, and Q_1 is turned OFF. As shown in Fig. 2(c), inductor L_1 is connected to B_2, and energy is transferred from L_1 to B_2. The inductor current i_L rises linearly, which is given by

$$i_L(t) = i_L(t_2)+\frac{V_{B2}}{R_1}\left(1-e^{-\frac{R_1}{L_1}(t-t_2)}\right). \quad (15)$$

The energy consumed by the internal resistance R_{B2} and R_1 during Mode III can be approximatively expressed as, respectively

$$E_{R_{B2}}(\mathrm{III}) \approx -\frac{1}{4}\cdot L_1\cdot i_L^2(t_2)\cdot\frac{R_{B2}}{R_1}\cdot\ln\left[1+\frac{R_1}{V_{B2}}\cdot i_L(t_2)\right] \quad (16)$$

$$E_{R1}(\mathrm{III}) \approx -\frac{1}{4}\cdot L_1\cdot i_L^2(t_2)\cdot\ln\left[1+\frac{R_1}{V_{B2}}\cdot i_L(t_2)\right]. \quad (17)$$

4) Mode IV [$t_3 - t_4$, Fig. 2(d)]: Q_2 keeps being turned ON, and Q_1 keeps being turned OFF. Mode IV does not start until the inductor current i_L rises to 0 at t_3. As shown in Fig. 2(d), the

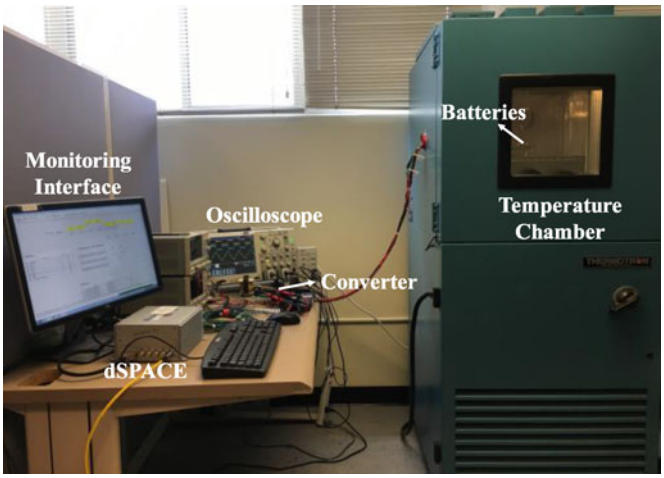

Fig. 4. Experiment setup.

inductor L_1 is charged by B_2, and energy is stored in inductor L_1. Based on KCL, the inductor current i_L can be calculated as

$$i_L(t) = \frac{V_{B2}}{R_1}\left(1 - e^{-\frac{R_1}{L_1}(t-t_3)}\right). \tag{18}$$

The energy consumed by the internal resistance R_{B2} and R_1 during Mode IV can be approximatively expressed as, respectively

$$E_{B2}(\mathrm{IV}) \approx -\frac{1}{4}\cdot L_1 \cdot i_L^2(t_4)\cdot \frac{R_{B2}}{R_1}\cdot \ln\left[1 - \frac{R_1}{V_{B2}}\cdot i_L(t_4)\right] \tag{19}$$

$$E_{R1}(\mathrm{IV}) \approx -\frac{1}{4}\cdot L_1 \cdot i_L^2(t_4)\cdot \ln\left[1 - \frac{R_1}{V_{B2}}\cdot i_L(t_4)\right]. \tag{20}$$

According to (16) and (19), the total energy used for heating B_2 during one switching period can be approximatively obtained as

$$E_{R_{B2}} \approx \frac{1}{4}\cdot\frac{L_1}{V_{B2}}\cdot R_{B2}\cdot[i_L^3(t_4) - i_L^3(t_2)]. \tag{21}$$

Similarly, it can be concluded that the heating speed of B_2 is proportional to the ac amplitudes $i_L(t_2)$ and $i_L(t_4)$ as well as the internal resistance R_{B2}.

The maximum energy stored in the inductor L_1 from cell B_2 at t_4 can be given by

$$E_{L1}(t_4) = \frac{1}{2}\cdot L_1 \cdot i_L^2(t_4). \tag{22}$$

It can be clearly seen that Mode I and Mode II achieve the ac charging and discharging for B_1, and Mode III and Mode IV obtain the ac charging and discharging for B_2. Moreover, during Modes II and III, energy is transferred from B_1 to B_2, and during Modes IV and I, energy is back-transferred from B_2 to B_1, ensuring energy balancing between the two cells.

Considering that $V_{B1} = V_{B2}$, it is easy to conclude that the duty cycle must be 50% for the energy balancing between the two cells in the steady state.

The conversion efficiency of the buck–boost converter can be calculated by the energy flowing out of a cell and the energy flowing into the cell. Thus, based on (8), (9), (12), and (14), considering that R_1 is smaller, the conversion efficiency for cell B_1 can be approximatively calculated as

$$\begin{aligned}\eta_{c,B1} &= \frac{E_{L1}(t_0) - E_{R1}(\mathrm{I}) - P_{\mathrm{Sloss}}\cdot T}{E_{L1}(t_2) + E_{R1}(\mathrm{II}) + P_{\mathrm{Sloss}}\cdot T} \\ &\approx \frac{\frac{1}{2}\cdot L_1\cdot i_L^2(t_0) - \frac{1}{4}\cdot\frac{L_1}{V_{B1}}\cdot R_1\cdot i_L^3(t_0) - P_{\mathrm{Sloss}}\cdot T}{\frac{1}{2}\cdot L_1\cdot i_L^2(t_2) - \frac{1}{4}\cdot\frac{L_1}{V_{B1}}\cdot R_1\cdot i_L^3(t_2) + P_{\mathrm{Sloss}}\cdot T} \\ &\quad\times 100\% \end{aligned} \tag{23}$$

where P_{Sloss} represents the switching loss, which can be calculated based on the datasheet of MOSFETs. Analogously, we can calculate the conversion efficiency for cell B_2. T is the switching period. From (23), it can be observed that the conversion efficiency depends mainly on the equivalent resistance R_1, the amplitude of the ac current, and the switching loss. The smaller the equivalent resistance R_1, the higher the conversion efficiency. Therefore, the components, such as MOSFET switches and inductors with low equivalent resistances, should be selected accordingly to satisfy the fine requirement of the heater. At lower frequencies, the switching loss is smaller and the resistive loss is larger. Considering that $i_L(t_0) \approx |i_L(t_2)|$, (23) can be further simplifies as

$$\eta_{c,B1} \approx \frac{2\cdot V_{B1} - i_L(t_0)\cdot R_1}{2\cdot V_{B1} - i_L(t_2)\cdot R_1}\times 100\%. \tag{24}$$

It can be seen that the lower the switching frequency, the larger the amplitude of the ac current, the lower the conversion efficiency. At higher frequencies, although the resistive loss become smaller, the switching loss is larger, which will also lead to a lower conversion efficiency. This shows that there exists an optimum frequency to maximize the conversion efficiency.

The heating efficiencies for B_1 and B_2 can be calculated by the energy consumed for heating the batteries and the energy consumed by the converter, which can be obtained as

$$\eta_{h,B1} = \eta_{h,B2} = \frac{R_B}{R_B + R_1}\times 100\%. \tag{25}$$

It can be seen that a larger internal resistance R_B and a smaller equivalent resistance R_1 will lead to a higher heating efficiency, which means more energy used for heating batteries.

The purpose of balancing is to transfer energy from the higher voltage cell to the lower voltage one. Thus, the balancing efficiency can be calculated as

$$\eta_e = \frac{V_{B2}\cdot\frac{|i_L(t_2)|+|i_L(t_4)|}{4}\cdot D - P_{N\mathrm{loss}}}{V_{B1}\cdot\frac{|i_L(t_0)|+|i_L(t_2)|}{4}\cdot(1-D) + P_{N\mathrm{loss}}}\times 100\% \tag{26}$$

where $P_{N\mathrm{loss}}$ is the inherent loss when there is no balancing between the two cells at $V_{B1} = V_{B2}$. It can be seen when the balancing power is larger, $P_{N\mathrm{loss}}$ can be neglected and (26) can be simplified as

$$\eta_e \approx \frac{V_{B2}\cdot\frac{|i_L(t_2)|+|i_L(t_4)|}{4}\cdot D}{V_{B1}\cdot\frac{|i_L(t_0)|+|i_L(t_2)|}{4}\cdot(1-D)}\times 100\% \approx \frac{V_{B2}}{V_{B1}}\times 100\%. \tag{27}$$

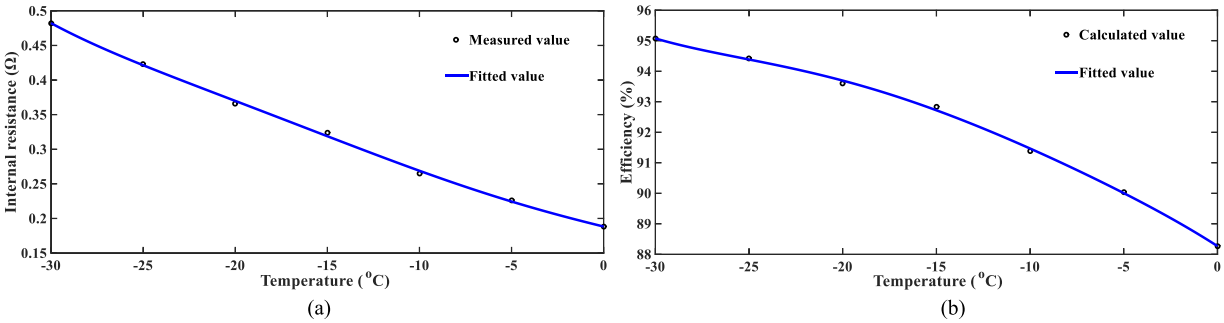

Fig. 5. (a) Internal resistance of a battery cell versus temperature. (b) Heating efficiency versus temperature.

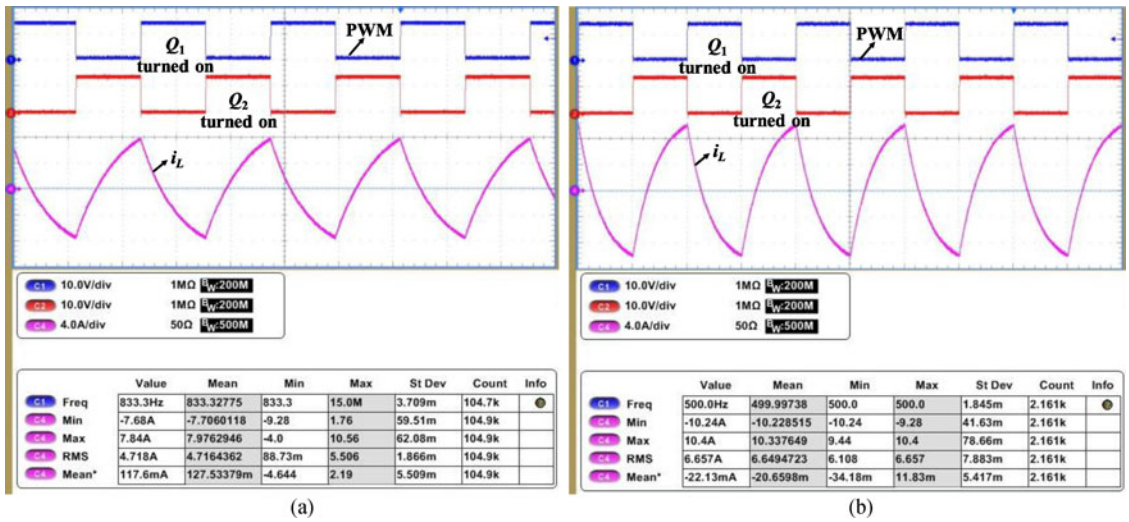

Fig. 6. Experimental waveforms of the proposed basic ac heater. (a) At $f = 833$ Hz. (b) At $f = 500$ Hz.

In this case, the balancing efficiency is inversely proportional to the voltage difference between the two cells. When the balancing power is smaller, the loss $P_{N\text{loss}}$ will account for a larger proportion of the balancing power, leading to a lower balancing efficiency. Therefore, the balancing efficiency first increases and then decreases along with the balancing power increasing.

According to the above analysis, it can be seen that the next-to-next heater has the same working modes as the basic one. Nevertheless, the operation principles of the interleaved parallel heater are somewhat complicated. The two conversion arms are, respectively, driven by a pair of complementary PWM signals with 180° phase shift angle and a duty cycle of 50%. Specifically, the synchronous switches Q_1 and Q_4 are turned ON during a half-cycle of a switching period, and the synchronous switches Q_2 and Q_3 are turned ON during the other half period. Thus, when the upper cell is heater by the first/second converter, the lower cell is simultaneously heated by the second/first converter. As a result, the batteries can be heated at all the time without rest, leading to a faster heating speed.

III. Experimental Results

For simplicity but without losing generality, the proposed heater is applied to two 2500-mAh $LiNiMnCoO_2$ cells and two 1100-mAh $LiFePO_4$ cells. Fig. 4 shows a photograph of the experiment setup. The switches $Q_1 - Q_2$ were implemented by STP220N6F7 MOSFETs with 2.4 mΩ internal resistance. The

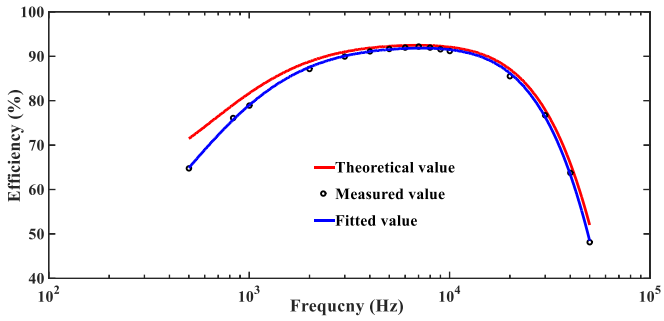

Fig. 7. Conversion efficiencies of the buck–boost converter as a function of switching frequency *f*.

measured equivalent resistance R_{L1} in the inductor is about 23 mΩ. The measured inductance L_1 was about 102.8 μH. Fig. 5(a) shows the internal resistances of the $LiNiMnCoO_2$ battery at different temperatures, which are measured by discharging the battery at 2 C. It can be seen that the lower the temperature, the larger the cell resistances. According to (25), Fig. 5(b) further shows the heating efficiencies at different temperatures, by which the average heating efficiency from −30 °C to 0 °C is calculated as 92.2%. The batteries were kept in the temperature chamber at the set temperatures for more than 3 h before preheating. The heating process ended when the battery temperature reached 0 °C or the heating time was beyond an hour.

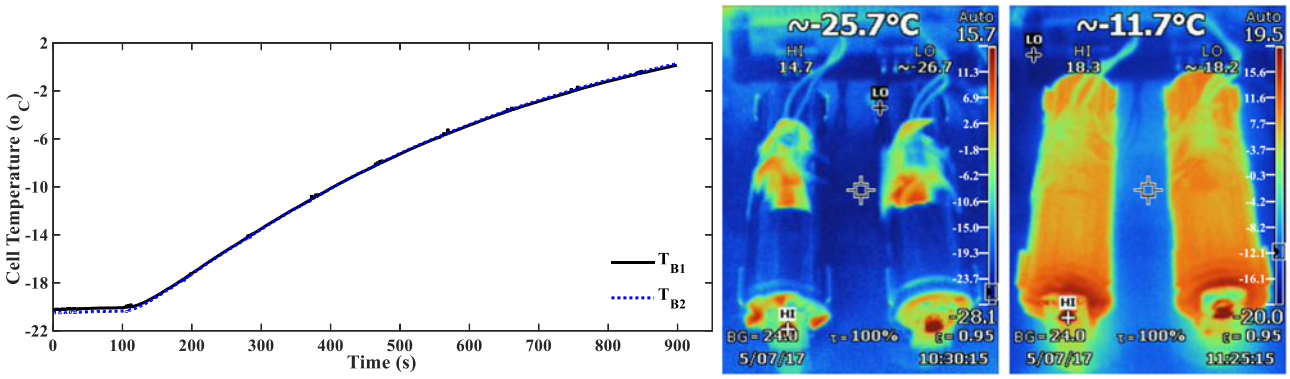

Fig. 8. Heating results of the basic topology for two $LiNiMnCoO_2$ cells with $f = 833$ Hz at -20 °C. (a) Temperature rises. (b) Cell temperature distributions before heating. (c) Cell temperature distributions after heating.

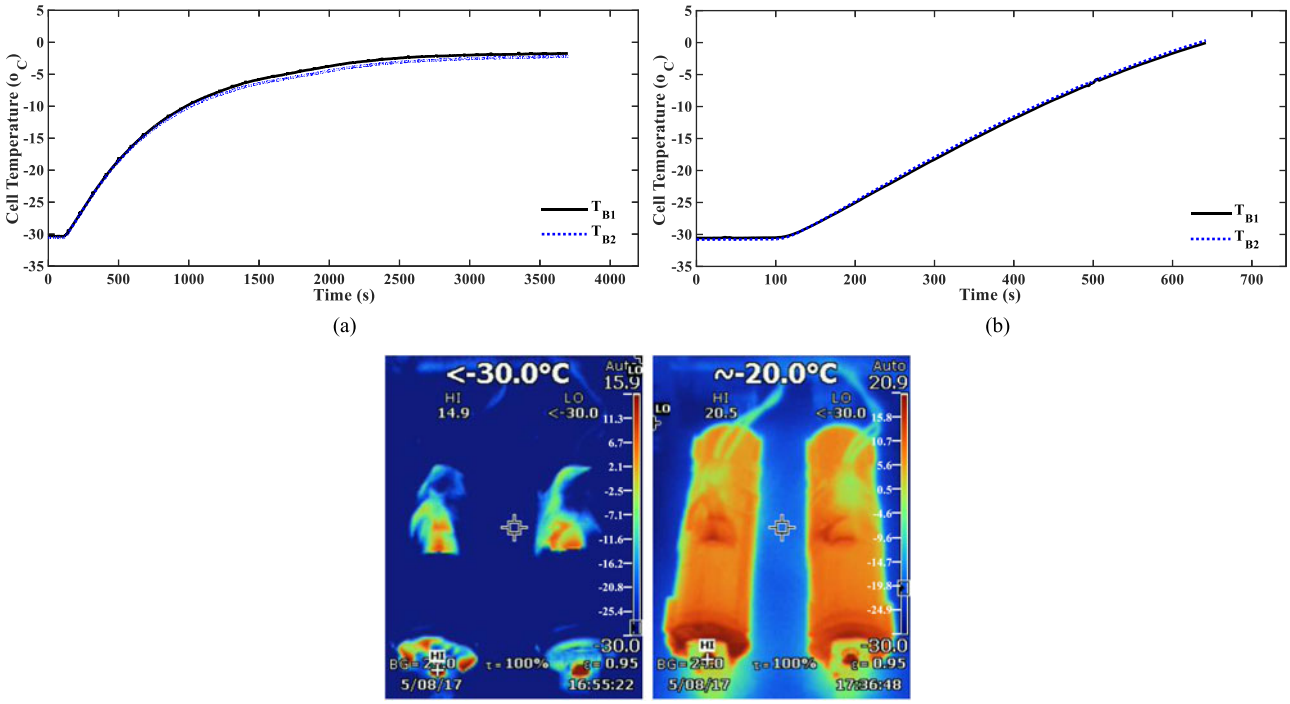

Fig. 9. Heating results of the basic topology for two $LiNiMnCoO_2$ cells at -30 °C. (a) Temperature rises at $f = 833$ Hz. (b) Temperature rises at $f = 500$ Hz. (c) Cell temperature distributions before heating at $f = 500$ Hz. (d) Cell temperature distributions after heating at $f = 500$ Hz.

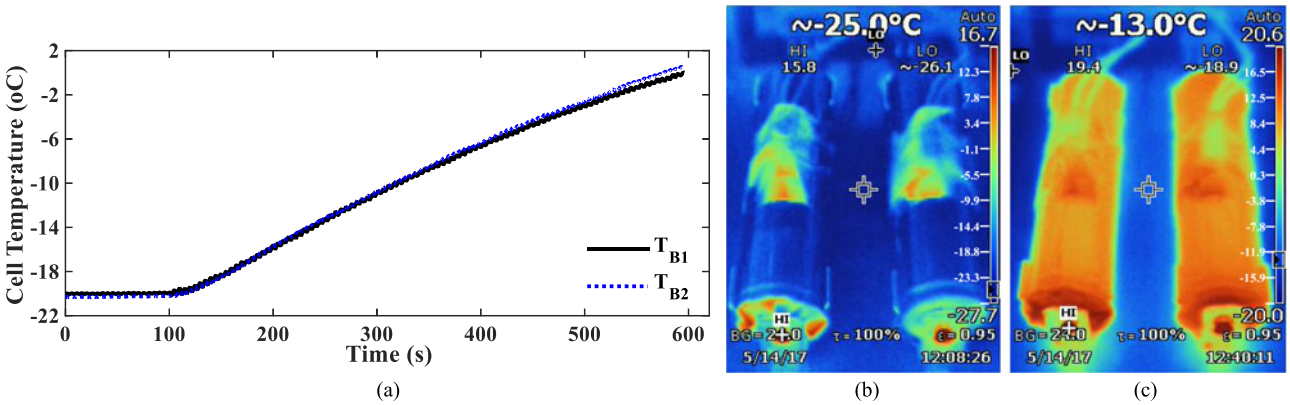

Fig. 10. Heating results of the basic topology for two $LiNiMnCoO_2$ cells with $f = 20$ kHz at -20 °C. (a) Temperature rises. (b) Cell temperature distributions before heating. (c) Cell temperature distributions after heating.

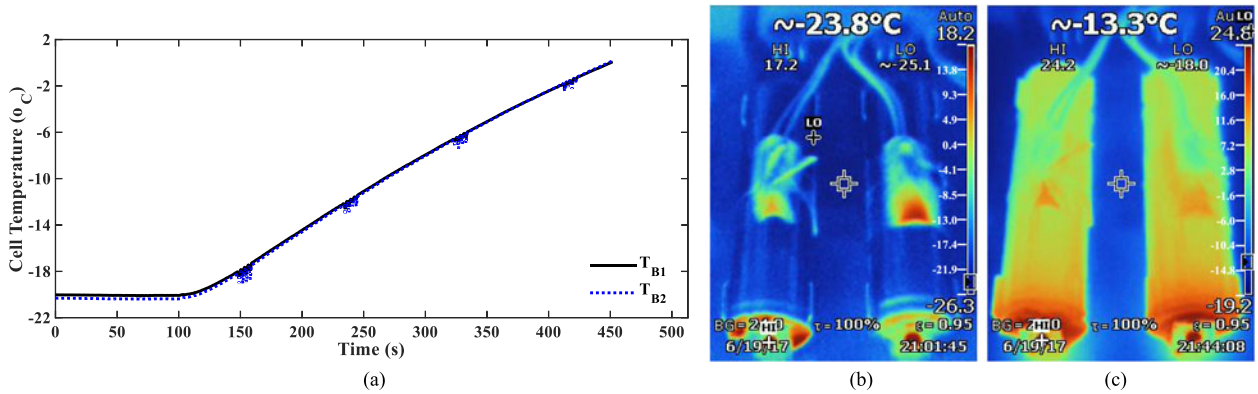

Fig. 11. Heating results of the interleaved-parallel-structured heater for two $LiNiMnCoO_2$ cells with $f = 833$ Hz at -20 °C. (a) Temperature rises. (b) Cell temperature distributions before heating. (c) Cell temperature distributions after heating.

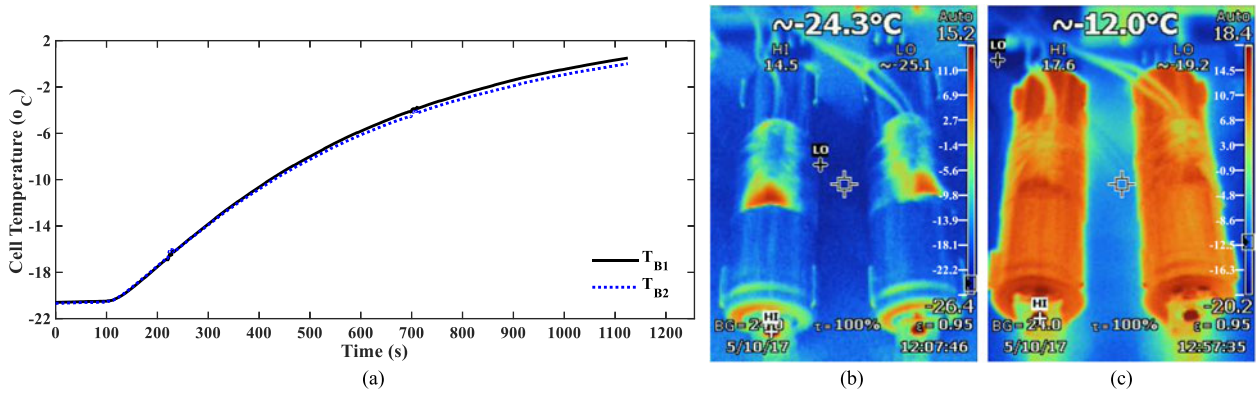

Fig. 12. Heating results of the basic topology for two $LiFePO_4$ cells with $f = 500$ Hz at -20 °C. (a) Temperature rises. (b) Cell temperature distributions before heating. (c) Cell temperature distributions after heating.

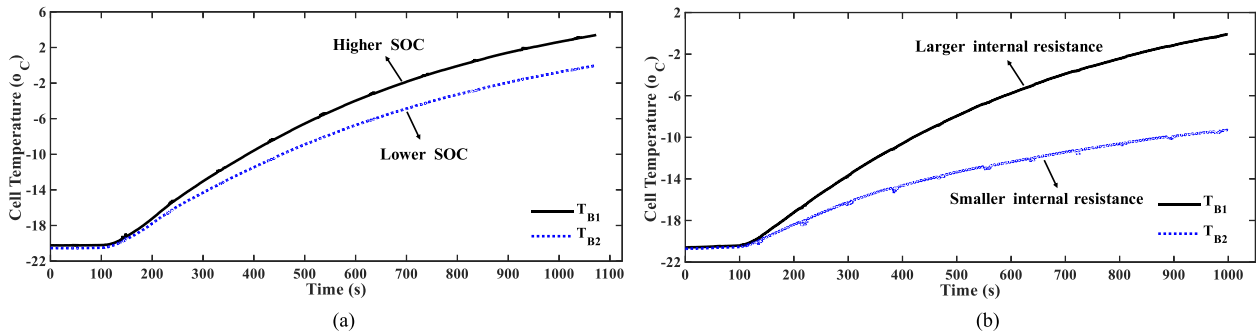

Fig. 13. Heating results for two unbalanced LiNiMnCoO2 cells with $f = 833$ Hz at -20 °C. (a) With unbalanced SOCs. (b) With unbalanced internal resistances.

Fig. 6 shows the experimental waveforms of the proposed ac heater at the frequencies of 833.3 and 500 Hz, respectively. It can be seen that the ac current is not the exact triangle waveform due to the impact of the larger battery internal resistances at low temperature. As shown in Fig. 6(a), at the frequency of $f =$ 833.3 Hz, the amplitude of the ac current is 7.8 A (3.1 C), and the rms heating current is 4.7 A (1.9 C). As shown in Fig. 6(b), when the frequency decreases to 500 Hz, the amplitude of the ac current is increased to 10.4 A (4.2 C) with the rms heating current increased to 6.7 A (2.7 C). These results show that the ac current amplitude can be regulated by controlling the switching frequency. Theoretically, with the same inductance, the lower the switching frequency, the larger the ac current amplitude. Thus, the heating speed subject to the ac current amplitude can be improved by decreasing the switching frequency.

Fig. 7 shows the measured conversion efficiency η_c as a function of the switching frequency. It can be seen that the conversion efficiency increases from 65.2% to 92.2% with the switching frequency increasing from 200 Hz to 7 kHz due to the decrease in the resistive loss. When the switching frequency increases from 7 to 50 kHz, η_c decreases from 92.2% to 48.2% due to the increase in the switching loss. It can be seen that the theoretical efficiency curve fits well with the measured conversion efficiencies. The small difference between the measured and theoretical

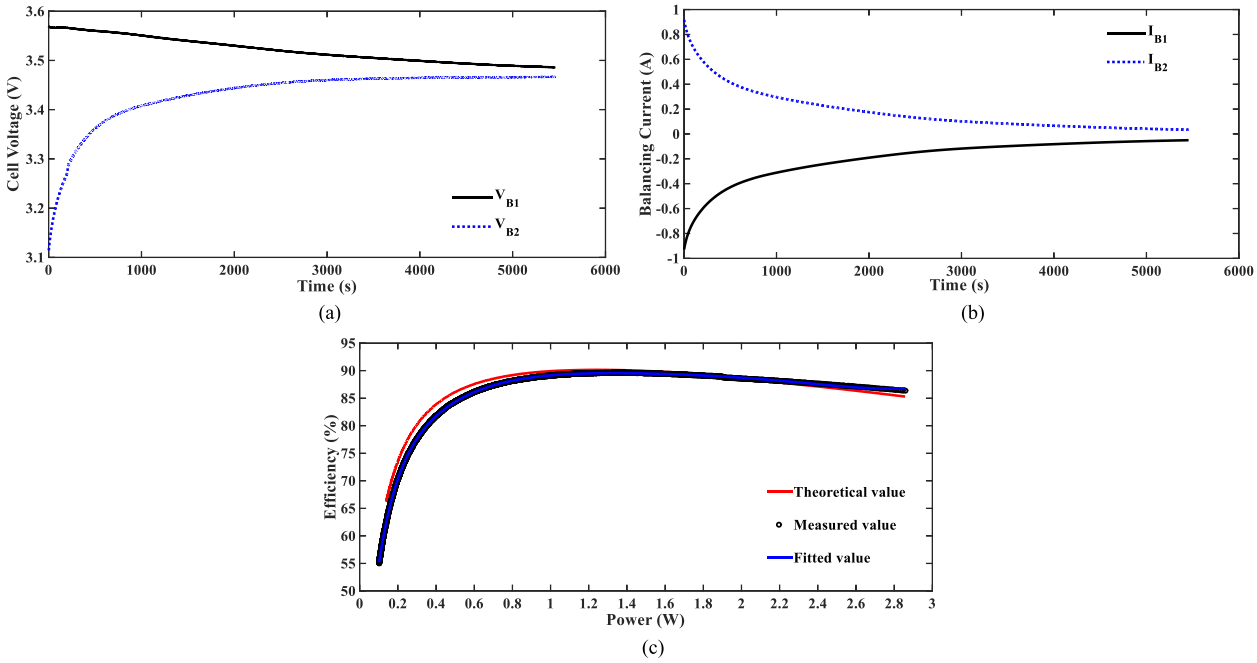

Fig. 14. Balancing results of the next-to-next topology for two $LiNiMnCoO_2$ cells with $f = 10$ kHz at room temperature. (a) Cell voltage trajectories versus time. (b) Cell current trajectories versus time. (c) Balancing efficiencies as a function of the output power.

balancing efficiencies is caused by the exponential behavior of the inductor current at lower frequencies.

In order to verify the validity of the proposed heater, Fig. 8 shows the heating results of the basic topology with the frequency of $f = 833$ Hz at -20 °C. As shown in Fig. 8(a), it can be observed that the cells are heated to 0 °C within 13 min by circulating an 833 Hz ac current with the amplitude of 7.8 A (3.1 C). The average temperature rise rate is 1.54 °C/min. About 7.1% cell energy is consumed during heating. As shown in Fig. 8(c), after heating, the surfaces of the two cells have the almost consistent temperature distributions, and the maximum temperature difference between the two cells is only 0.3 °C, showing a good heating uniformity.

Fig. 9 shows the heating results for two $LiNiMnCoO_2$ cells at -30 °C. As shown in Fig. 9(a), at 833 Hz, the heating time is longer than an hour or the cells cannot be heated to 0 °C. To speed up the heating process, the switching frequency is decreased to 500 Hz, and the amplitude of the ac current is increased to 4.2 C. As shown in Fig. 9(b), the heating time is reduced to 9 min to heat the cells to above 0 °C with about 7.7% cell energy loss. The average temperature rise rate reaches 3.33 °C/min. Fig. 9(c) and (d) shows the good heating uniformity for the two cells. It can be concluded that with the same inductance, the heating speed can be significantly increased by decreasing the switching frequency.

Fig. 10 shows the heating results of the basic topology at $f = 20$ kHz with the same amplitude of ac current as that at 833 Hz. The inductance L_1 is determined as 1.9 μH. As shown in Fig. 10(a), due to the higher frequency ac heating, the heating time is reduced to 8.3 min, shortened by 36.2% compared with the result at 833 Hz. The average temperature rise rate reaches 2.4 °C/min. About 6.7% cell energy loss is consumed during heating. It can be found that with the same ac current amplitude, the heating speed can be also improved by increasing the switching frequency.

Fig. 11 shows the heating results of the interleaved-parallel-structured heater with the same experimental conditions compared with Fig. 8. Due to the "all-time" heating for batteries, the heating time is only 5.9 min, dramatically shortened by 54.6%, with less energy loss, *i.e.*, about 5% compared with the basic topology. Moreover, the average temperature rise rate reaches 3.4 °C/min.

In order to prove the validity of the proposed heater for other kinds of batteries, Fig. 12 shows the heating results of the basic topology for two $LiFePO_4$ cells at -20 °C. The switching frequency is set as 500 Hz and the rms ac current is about 5.8 C. It takes 18 min to heat the cells to above 0 °C with a good heating uniformity. Due to the lower cell voltages and different battery materials, the heating for $LiFePO_4$ cells is slower than $LiNiMnCoO_2$ cells, which needs a larger ac current to circulate though $LiFePO_4$ batteries.

Fig. 13 shows the heating results for two unbalanced cells with $f = 833$ Hz at -20 °C. It can be found that the unbalance in SOCs or internal resistances will cause a large temperature difference, e.g., 3.5 °C in Fig. 13(a) and 9.3 °C in Fig. 13(b), between the two cells. Therefore, cells should be kept being balanced as much as possible to achieve the synchronous heating.

Fig. 14 shows the balancing results for two $LiNiMnCoO_2$ cells with a higher switching frequency of $f = 10$ kHz at room temperature. As shown in Fig. 14(a), the initial maximum voltage gap between cells is 452 mV. After 3500 s, the cell voltages are almost balanced with a small voltage gap of 18 mV between the two cells. Fig. 14(b) shows the balancing currents, which becomes smaller and smaller along with the balancing. Fig. 14(c) shows the theoretical and measured efficiencies as a function of the balancing power. It can be seen that the theoretical balancing

efficiency agrees well with the measured efficiency. When the balancing power increases from 0.10 to 1.36 W, the measured efficiency increases from 55.2% to 89.6%. When the balancing power increases from 1.36 to 2.86 W, the measured efficiency decreases from 89.6% to 86.4%. These results show that the proposed topology can also balance cell voltages at a higher switching frequency.

IV. Conclusion

The purpose of this paper is to introduce an automotive onboard ac heater without requiring external heating devices and power supplies for lithium-ion batteries at low temperatures, which can meet the application requirements of EVs for performance, reliability, size, and cost. Three heating topologies are introduced, *i.e.*, the basic, interleaved parallel, and next-to-next heaters. The configurations of the proposed heaters, operation principles, heating performances, and balancing verification are presented. It is first proved that it is fully feasible for batteries to provide enough energy to heat themselves without the need of any external power supplies and devices. Experimental results demonstrate:

1) The proposed systems achieve the effective heating for lithium-ion batteries with a fast speed, high efficiency, good uniformity, and strong robustness.
2) With the same inductance, the heating speed can be significantly increased by decreasing the switching frequency.
3) With the same current amplitude, the heating speed can be also improved by increasing the switching frequency.
4) The unbalance in SOCs or internal resistances will cause a large temperature difference between cells.
5) The proposed interleaved parallel heater achieves a higher heating speed and efficiency without causing more harm to the batteries compared with the basic topology.
6) Except heating, the next-to-next topology can also automatically balance cell voltages with the same control at a higher frequency without the requirement of additional balancing circuits, increasing the power density of BMSs.
7) The proposed ac heaters can be applied to other rechargeable batteries without any change or recalibration.

In conclusion, with the proposed heater, "all-climate" and "all-voltage" battery packs can be easily achieved without changing battery structures and electrolytes, which is of great significance to the rapid development of EVs. In the future, the heat generated in MOSFETs due to the switching loss and conduction loss will be utilized to heat batteries externally to further improve the heating speed and efficiency.

References

[1] D.-H. Kim, M.-J. Kim, and B.-K. Lee, "An integrated battery charger with high power density and efficiency for electric vehicles," *IEEE Trans. Power Electron.*, vol. 32, no. 6, pp. 4553–4565, Jun. 2017.

[2] AAA Newsroom, Heathrow, FL, USA, "Extreme temperatures affect electric vehicle driving range," Mar. 2014. [Online]. Available: http://newsroom.aaa.com/2014/03/extreme-temperatures-affect-electric-vehicle-driving-range-aaa-says/. Accessed on: Apr. 23, 2017.

[3] M. Armand and J.-M. Tarascon, "Building better batteries," *Nature*, vol. 451, no. 7179, pp. 652–657, Feb. 2008.

[4] Y. Ji, Y. Zhang, and C.-Y. Wang, "Li-ion cell operation at low temperatures," *J. Electrochem. Soc.*, vol. 160, no. 4, pp. 636–649, Feb. 2013.

[5] S. Zhang, K. Xu, and T. Jow, "The low temperature performance of Li-ion batteries," *J. Power Sources*, vol. 115, no. 1, pp. 137–140, Mar. 2003.

[6] S. S. Zhang, K. Xu, and T. R. Jow, "Electrochemical impedance study on the low temperature of Li-ion batteries," *Electrochim. Acta*, vol. 49, no. 7, pp. 1057–1061, Mar. 2004.

[7] L. Liao *et al.*, "Effects of temperature on charge/discharge behaviors of $LiFePO_4$ cathode for Li-ion batteries," *Electrochim. Acta*, vol. 60, pp. 269–273, Jan. 2012.

[8] S. Mohan, Y. Kim, and A. G. Stefanopoulou, "Energy-conscious warm-up of li-ion cells from subzero temperatures," *IEEE Trans. Ind. Electron.*, vol. 63, no. 5, pp. 2954–2964, May 2016.

[9] Z. Lei, C. Zhang, J. Li, G. Fan, and Z. Lin, "Preheating method of lithium-ion batteries in an electric vehicle," *J. Modern Power Syst. Clean Energy*, vol. 2, no. 2, pp. 289–296, Jun. 2015.

[10] A. A. Pesaran, "Battery thermal management in EVs and HEVs: Issues and solutions," in *Proc. Adv. Automot. Battery Conf.*, 2001, pp. 1–10.

[11] A. Pesaran, A. Vlahinos, and T. Stuart, "Evaluation of heating methods for HEV batteries for cold seasons," Nat. Renewable Energy Lab., Golden, CO, USA, NREL Milestone Rep., Aug. 2001.

[12] Y. Ji and C. Y. Wang, "Heating strategies for Li-ion batteries operated from subzero temperatures," *Electrochim. Acta*, vol. 107, pp. 664–674, Sep. 2013.

[13] C. Ashtiani and T. Stuart, "Circulating current battery heater," U.S. Patent 6 259 229, Jul. 2001.

[14] S. Mohan, J. Siegel, A. G. Stefanopoulou, M. Castanier, and Y. Ding, "Synthesis of an energy-optimal self-heating strategy for Li-ion batteries," in *Proc. IEEE Decision Control*, 2016, pp. 1589–1594.

[15] A. Vlahinos and A. A. Pesaran, "Energy efficient battery heating in cold climates," Soc. Automot. Eng., Warrendale, PA, USA, Tech. Paper 2002-01-1975, 2002.

[16] A. Pesaran, A. Vlahinos, and T. Stuart, "Cooling and preheating of batteries in hybrid electric vehicles," in *Proc. 6th ASME-JSME Thermal Eng. Joint Conf.*, 2003, pp. 1–7.

[17] J. Zhang, H. Ge, Z. Li, and Z. Ding, "Internal heating of lithium-ion batteries using alternating current based on the heat generation model in frequency domain" *J. Power Sources*, vol. 273, pp. 1030–1037, Jan. 2015.

[18] H. Ruan *et al.*, "A rapid low-temperature internal heating strategy with optimal frequency based on constant polarization voltage for lithium-ion batteries," *Appl. Energy*, vol. 177, pp. 771–782, Sep. 2016.

[19] C.-Y. Wang *et al.*, "Lithium-ion battery structure that self-heats at low temperatures," *Nature*, vol. 529, no. 7587, pp. 515–518, Jan. 2016.

[20] G. Zhang, S. Ge, T. Xu, X.-G. Yang, H. Tian, and C.-Y. Wang, "Rapid self-heating and internal temperature sensing of lithium-ion batteries at low temperatures," *Electrochim. Acta*, vol. 218, pp. 149–155, Nov. 2016.

[21] X.-G. Yang, G. Zhang, and C.-Y. Wang, "Computational design and refinement of self-heating lithium ion batteries," *J. Power Sources*, vol. 328, pp. 203–211, Oct. 2016.

[22] T. A. Stuart and A. Hande, "HEV battery heating using AC currents," *J. Power Sources*, vol. 129, pp. 368–378, Apr. 2004.

[23] T. H. Phung, A. Collet, and J.-C. Crebier, "An optimized topology for next-to-next balancing of series-connected lithium-ion cells," *IEEE Trans. Power Electron.*, vol. 29, no. 9, pp. 4603–4613, Sep. 2014.

Yunlong Shang (S'14) received the B.S. degree in automation from Hefei University of Technology, Hefei, China, in 2008 and the Ph.D. degree in control theory and control engineering from Shandong University, Jinan, China, in 2017. Between Sep. 2015 and Oct. 2017, he conducted scientific research as a joint Ph.D. student in the DOE GATE Center for Electric Drive Transportation at San Diego State University, San Diego, CA, USA.

Since 2017, he has been working as a Postdoctor Research Fellow in the Department of Electrical and Computer Engineering, San Diego State University. His current research interests include the design and control of battery management systems and battery equalizers, battery modeling, and battery state estimation.

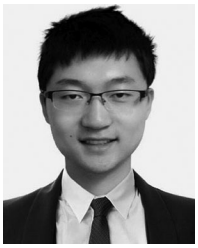

Bing Xia (S'13) received the B.S. degree in mechanical engineering from the University of Michigan, Ann Arbor, MI, USA and the B.S. degree in electrical engineering from Shanghai Jiaotong University, Shanghai, China, in 2012. Between winter 2013 and summer 2015, he was a Ph.D. student in automotive system engineering at the University of Michigan—Dearborn, Dearborn, MI. Since fall 2015, he has been working toward the Ph.D. degree in the joint Ph.D. program at San Diego State University, San Diego, CA, USA and University of California San Diego, La Jolla, CA.

His research interests include batteries, including charging optimization, battery safety, and battery management.

Naxin Cui (M'14) received the B.S. degree in automation from Tianjin University, Tianjin, China, in 1989, and the M.S. and Ph.D. degrees in control theory and applications from Shandong University, Jinan, China, in 1994 and 2005, respectively.

In 1994, she joined Shandong University, where she is currently a Full Professor in the School of Control Science and Engineering. Her current research interests include power electronics, motor drives, automatic control theory and application, and battery energy management systems of electric vehicles.

Chenghui Zhang (M'14–SM'17) received the Bachelor's and Master's degrees in automation engineering from Shandong University of Technology, Jinan, China, in 1985 and 1988, and the Ph.D. degree in control theory and operational research from Shandong University, Jinan, in 2001.

In 1988, he joined Shandong University, where he is currently a Professor in the School of Control Science and Engineering, the Chief Manager of Power Electronic Energy-Saving Technology & Equipment Research Center of the Education Ministry, a Cheung Kong Scholars Professor specially invited by China's Ministry of Education, and a Taishan Scholar Special Adjunct Professor. He is also one of the State-level candidates of "the New Century National Hundred, Thousand and Ten Thousand Talent Project," the academic leader of the Innovation Team of the Ministry of Education, and the Chief Expert of the National "863" high technological planning. His research interests include optimal control of engineering, power electronics and motor drives, energy-saving techniques, and time-delay systems.

Chunting Chris Mi (S'00–A'01–M'01–SM'03–F'12) received the B.S.E.E. and M.S.E.E. degrees in electrical engineering from Northwestern Polytechnical University, Xi'an, China, in 1985 and 1988, respectively, and the Ph.D. degree in electrical engineering from the University of Toronto, Toronto, ON, Canada, in 2001.

He is a Professor and Chair of electrical and computer engineering, and the Director of the Department of Energy-funded Graduate Automotive Technology Education Center for Electric Drive Transportation, San Diego State University (SDSU), San Diego, CA, USA. Prior to joining SDSU, he was with with the University of Michigan, Dearborn from 2001 to 2015. He has conducted extensive research and has authored or coauthored more than 100 journal papers. His research interests include electric drives, power electronics, electric machines, renewable-energy systems, and electrical and hybrid vehicles.